

**Suggestions for revision or reasons for rejection (will be published if the paper is accepted for final publication)**

Dear authors,

1. In my initial assessment I raised 4 main points concerning methods and data handling, representation of uncertainty and validation. I am happy to say that you have well dressed most of the points raised. In particular, I appreciate that you now add uncertainties to all numbers (I suggest to even remove "mildly increased" based on the uncertainty). Furthermore data handling is much clearer now. Lastly, thank you for adding the cruise information from SOCAT.

**Response:** We agree with the reviewer's suggestion and have removed 'mildly'.

Overall, I believe the manuscript is technically sound and the results are well put in context. Therefore, I think the manuscript can be published after fixing a few remaining issues:

2. **Methods:** While the language is much simpler now and readability has improved, it still reads very difficult and it is certainly still the weakest bit. It is important for the reader to know why the inputs are in vector form. Between what are Euklidian distances calculated? What is a winning neuron? Maybe add a simple example with real data. Imagine an input vector (now with values I made up) with SST=3, SSS=32, CHI=1, MLD=10 and 2 neurons on the map with values (4,30,0.5,5) and (5,35,0,100) respectively. What is the winning neuron? after you have identified the winning neuron, what happens in step 1? and what happens in step 2? Then the link to the geography is also more visible, because the input vector values belong to a certain point in space, etc. That would be my suggestion here.

**Response:** Because during the first step, each neuron's weight vectors, which are linearly initialized, are repeatedly trained by being presented with the input vectors. The inputs are prepared in vector form. We have added more explanation in our manuscript. More detailed procedure comes from Nakaoka et al., 2013, we have added this reference in the text. We have added the equation to calculate the Euclidean distances to select a winner neuron as Eq.2 and added the explanation in the manuscript.

3. On line 142-144 I read: "The solubility of CO<sub>2</sub> is affected by temperature and salinity in the water as well as biological activities, such as phytoplankton taking up CO<sub>2</sub> through photosynthesis and organisms releasing CO<sub>2</sub> through respiration (Chen et al., 2011)." - I suppose this is a mistake from the authors (maybe awkward phrasing) as biology is not influencing the solubility.

**Response:** We have rephrased this part.

4. Throughout the manuscript spaces are missing (see as example abstract line 15 and line 27 last word(s) of the line. This is reoccurring but nothing major.

**Response:** It is a version problem. When our manuscript is opened in Word 2016 it is OK however when it is opened in other version the problem will occur. We have saved our manuscript to be in doc instead of docx and hope it will be OK.

5. lines 31-32: This is still awkwardly phrased as carbon uptake implies that the flux is from (and not "to or from") the atmosphere. Best is to remove the phrase "during the transport of CO<sub>2</sub> to or from the atmosphere" as a whole.

**Response:** It has been removed.

6. line 88: satellites actually do measure CO<sub>2</sub> now - just not in the ocean (see GO-sat or OCO-2). So please say "measure sea surface pCO<sub>2</sub>"

**Response:** We have changed it.

7. line 139: remove of carbon cycling.

**Response:** It has been removed.

8. line 169-170: please add a reference of some more text on the different methods. (better a reference)

**Response:** A reference about different methods to calculate MLD has been added.

9. line 250: explain the Kriging method? or add a reference

**Response:** The Kriging method we use is in SURFER software (version 7.3.0.35) and we have added it in the manuscript.

10. line 473: replace "could be" with "can be" - you just did.

**Response:** It has been replaced.

# Variations in the Summer Oceanic $p\text{CO}_2$ and Carbon Sink in the Prydz Bay Using the SOM Analysis Approach

Suqing Xu<sup>1</sup>, Keyhong Park<sup>2\*</sup>, Yanmin Wang<sup>3</sup>, Liqi Chen<sup>1\*</sup>, Di Qi<sup>1</sup>, Bingrui Li<sup>4</sup>

1. Key Laboratory of Global Change and Marine-Atmospheric Chemistry, Third Institute of Oceanography, Xiamen 361005, PR China.
2. Division of Polar Ocean Sciences, Korea Polar Research Institute, Incheon 21990, South Korea.
3. Haikou Marine Environment Monitoring Central Station, State Oceanic Administration, Haikou 570100, China.
4. Polar Research Institute of China, Shanghai 200136, China.

Correspondence to: Liqi Chen ([chenliqi@tio.org.cn](mailto:chenliqi@tio.org.cn));

Keyhong Park ([keyhongpark@kopri.re.kr](mailto:keyhongpark@kopri.re.kr))

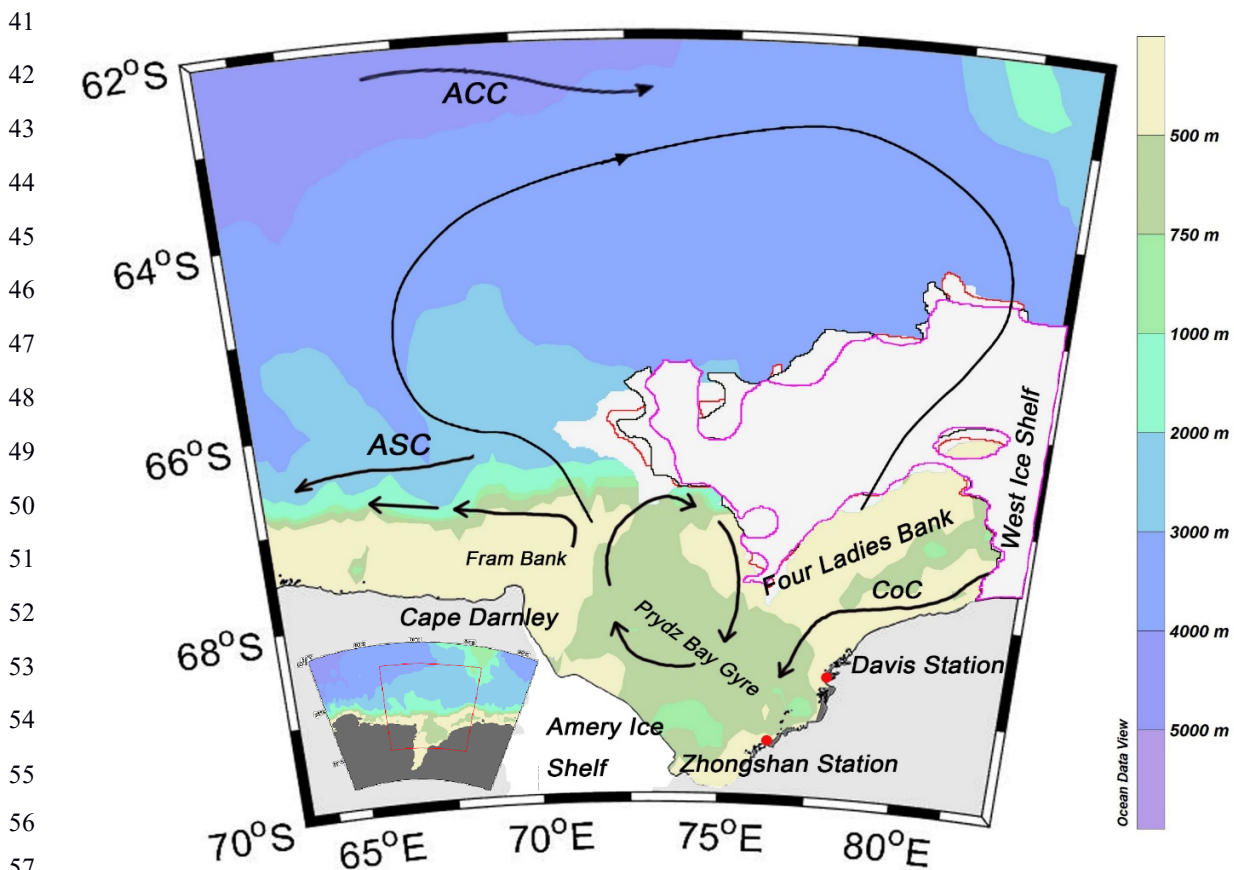
## Abstract

This study applies a neural network technique to produce maps of oceanic surface  $p\text{CO}_2$  in the Prydz Bay in the Southern Ocean on a weekly  $0.1^\circ$  longitude  $\cdot$   $0.1^\circ$  latitude grid based on in situ measurements obtained during the 31<sup>st</sup> CHINARE cruise from February to early March of 2015. This study area was divided into three regions, namely, the Open-ocean region, Sea-ice region and Shelf region. The distribution of oceanic  $p\text{CO}_2$  was mainly affected by physical processes in the Open-ocean region, where mixing and upwelling were the main controls. In the Sea-ice region, oceanic  $p\text{CO}_2$  changed sharply due to the strong change in seasonal ice. In the Shelf region, biological factors were the main control. The weekly oceanic  $p\text{CO}_2$  was estimated using a self-organizing map (SOM) with four proxy parameters (Sea Surface Temperature, Chlorophyll-a concentration, Mixed Layer Depth, and Sea Surface Salinity) to overcome the complex relationship between the biogeochemical and physical conditions in the Prydz Bay region. The reconstructed oceanic  $p\text{CO}_2$  data coincide well with the in situ investigated  $p\text{CO}_2$  data from SOCAT, with a root-mean-square error of  $22.14 \mu\text{atm}$ . The Prydz Bay was mainly a strong  $\text{CO}_2$  sink in February 2015, with a monthly averaged uptake of  $23.57 \pm 6.36 \text{ TgC}$ . The oceanic  $\text{CO}_2$  sink is pronounced in the Shelf region due to its lowest oceanic  $p\text{CO}_2$  and peak biological production.

29 **1 Introduction**

30 The amount of carbon uptake occurring in the ocean south of 60°S during the transport of CO<sub>2</sub>  
31 to or from the atmosphere is still uncertain despite its importance in regulating atmospheric carbon  
32 and acting as a net sink for anthropogenic carbon (Sweeney et al., 2000, 2002; Morrison et al.,  
33 2001; Sabine et al., 2004; Metzl et al., 2006; Takahashi et al., 2012). This uncertainty arises from  
34 both the strong seasonal and spatial variations that occur around Antarctica and the difficulty of  
35 obtaining field measurements in the region because of its hostile weather and remoteness.

36 Following the Weddell and Ross seas, the Prydz Bay is the third-largest embayment in the  
37 Antarctic continent. Situated in the Indian Ocean section, the Prydz Bay is located close to the  
38 Amery Ice Shelf to the southwest and the West Ice Shelf to the northeast, with Cape Darnley to the  
39 west and the Zhongshan and Davis stations to the east (Fig. 1). In this region, the water depth  
40 increases sharply northward from 200 m to 3000 m.



58 Fig. 1 Ocean circulations in the Prydz Bay derived from Roden et al. (2013)-, Sun et al. (2013), Wu et al. (2017).  
59 ASC: Antarctic Slope Current; CoC: Antarctic Coastal Current; ACC: Antarctic Circumpolar Current. During

60 the 4-week cruise, the sea ice extent varied as indicated by the contoured white areas: the pink line is for  
61 week-1(20150202-20150209), the black line is for week-2 (20150210-20150217), the red line is for the week-3  
62 (20150218-20150225) and a fourth contoured area is for week-4 (20150226-20150305).

63 The inner continental shelf is dominated by the Amery Depression, which mostly ranges in  
64 depth from 600 to 700 m. This depression is bordered by two shallow banks (<200 m): the Fram  
65 Bank and the Four Ladies Bank, which form a spatial barrier for water exchange with the outer  
66 oceanic water (Smith and Trégure, 1994). The Antarctic Coastal Current (CoC) flows westward,  
67 bringing in cold waters from the east. When the CoC reaches the shallow Fram Bank, it turns  
68 north and then partly flows westward, while some of it turns eastward, back to the inner shelf,  
69 resulting in the clockwise-rotating Prydz Gyre (see Fig.1). The circulation to the north of the bay  
70 is characterized by a large cyclonic gyre, extending from within the bay to the Antarctic  
71 Divergence at approximately 63°S (Nunes Vaz and Lennon, 1996; Middleton and Humphries,  
72 1989; Smith et al., 1984; Roden et al., 2013; Wu et al., 2017). The inflow of this large gyre hugs  
73 the eastern rim of the bay and favours the onshore intrusions of warmer modified Circumpolar  
74 Deep Water across the continental shelf break (Heil et al., 1996). Westward flow along the shelf,  
75 which is part of the wind-driven Antarctic Slope Current (ASC), supplies water to the Prydz Bay.

76 It has been reported that the Prydz Bay is a strong carbon sink, especially in the austral  
77 summer (Gibson et al., 1999; Gao et al., 2008; Roden et al., 2013). Moreover, studies have  
78 shown that the Prydz Bay region is one of the source regions of Antarctic Bottom Water as well  
79 as the Weddell and Ross seas (Jacobs and Georgi, 1977; Yabukiet al., 2006). It is thus important  
80 to study the carbon cycle in the Prydz Bay. However, the analysis of the temporal variability and  
81 spatial distribution mechanism of oceanic  $p\text{CO}_2$  in the Prydz Bay is limited to cruises or stations  
82 due to its unique physical environment and complicated marine ecosystem (Smith et al., 1984;  
83 Nunes Vaz et al., 1996; Liu et al., 2003). To estimate regional sea-air  $\text{CO}_2$  fluxes, it is necessary to  
84 interpolate between in situ measurements to obtain maps of oceanic  $p\text{CO}_2$ . Such an interpolation  
85 approach, however, is still difficult, as observations are too sparse over both time and space to  
86 capture the high variability in  $p\text{CO}_2$ . Satellites do not measure [sea surface](#)  $p\text{CO}_2$ , but they do  
87 provide access to the parameters related to the processes that control its variability. The seasonal  
88 and geographical variability of surface water  $p\text{CO}_2$  is indeed much greater than that of atmospheric  
89  $p\text{CO}_2$ . Therefore, the direction of sea-air  $\text{CO}_2$  transfer is mainly regulated by oceanic  $p\text{CO}_2$ , and  
90 the method of spatially and temporarily interpolating in situ measurements of oceanic  $p\text{CO}_2$  has  
91 long been used (Takahashi et al., 2002 and 2009; Olsen et al., 2004; Jamet et al., 2007; Chierici et

92 al., 2009). In earlier studies, a linear regression extrapolation method was applied to expand cruise  
93 data to study the carbon cycle in the Southern Ocean (Rangama et al., 2005; Chen et al., 2011; Xu  
94 et al., 2016). However, this linear regression relied simply on either chlorophyll-a (CHL) or sea  
95 surface temperature (SST) parameters. Thus, this method can not sufficiently represent all  
96 controlling factors. In this study, we applied self-organizing map (SOM) analysis to expand our  
97 observed data sets and estimate the oceanic  $p\text{CO}_2$  in the Prydz Bay from February to early March  
98 of 2015.

99 The SOM analysis, which is a type of artificial neural network, has been proven to be a useful  
100 method for extracting and classifying features in the geosciences, such as trends in (and between)  
101 input variables (Gibson et al., 2017; Huang et al., 2017b). The SOM uses an unsupervised  
102 learning algorithm (i.e., with no need for a priori, empirical or theoretical descriptions of  
103 input-output relationships), thus enabling us to identify the relationships between the state  
104 variables of the phenomena being analysed, where our understanding of these cannot be fully  
105 described using mathematical equations and thus where applications of knowledge-based models  
106 are limited (Telszewski et al., 2009). In the field of oceanography, SOM has been applied for the  
107 analysis of various properties of seawater, such as sea surface temperature (Iskandar, 2010; Liu et  
108 al., 2006), and chlorophyll concentration (Huang et al., 2017a; Silulwane et al., 2001). In the past  
109 decade, SOM has also been applied to produce basin-scale  $p\text{CO}_2$  maps, mainly in the North  
110 Atlantic and Pacific Ocean, by using different proxy parameters (Lafevre et al., 2005; Friedrich  
111 & Oeschies, 2009a, 2009b; Nakaoka et al., 2013; Telszewski et al., 2009; Hales et al., 2012; Zeng et  
112 al., 2015; Laruelle et al., 2017). SOM has been proven to be useful for expanding the  
113 spatial-temporal coverage of direct measurements or for estimating properties whose satellite  
114 observations are technically limited. One of the main benefits of the neural network method over  
115 more traditional techniques is that it provides more accurate representations of highly variable  
116 systems of interconnected water properties (Nakaoka et al., 2013).

117 We conducted a survey during the 31<sup>st</sup> CHINARE cruise in the Prydz Bay (Fig. 2). This study  
118 aimed to apply the SOM method, combined with remotely sensed data, to reduce the  
119 spatiotemporal scarcity of contemporary  $\Delta p\text{CO}_2$  data and to obtain a better understanding of the  
120 capability of carbon absorption in the Prydz Bay from 63°E to 83°E and 64°S to 70°S from  
121 February to early March of 2015.

122 The paper is organized as follows. Section 2 provides descriptions of the in situ measurements  
123 and SOM methods. Section 3 presents the analysis and discussion of the results, and section 4  
124 presents a summary of this research.

## 125 **2 Data and methods**

### 126 **2.1 In situ data**

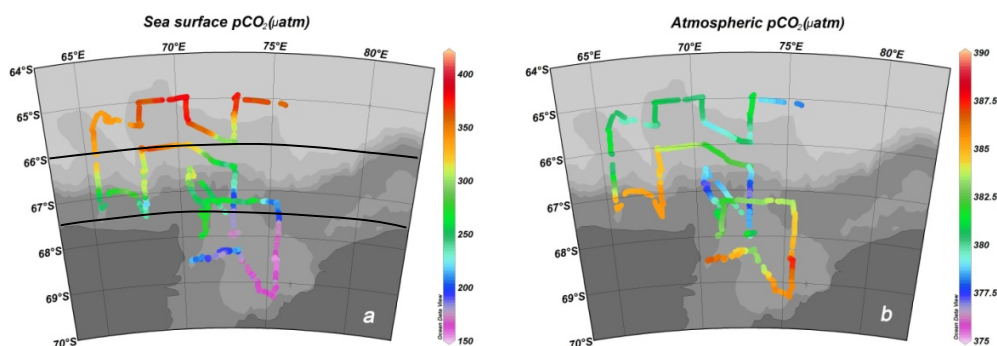
127 The in situ underway  $p\text{CO}_2$  values of marine water and the atmosphere were collected during  
128 the 31<sup>st</sup> CHINARE cruise, when the R/V Xuelong sailed from east to west from the beginning of  
129 February to early March, 2015 (see Fig.2a, b). Sea water at a depth of 5 metres beneath the sea  
130 surface was pumped continuously to the GO system (GO Flowing  $p\text{CO}_2$  system, General Oceanics  
131 Inc., Miami FL, USA), and the partial pressure of the sea surface water was measured by an  
132 infrared analyser (LICOR, USA, Model 7000). The analyser was calibrated every 2.5-3 h using  
133 four standard gases supplied by NOAA's Global Monitoring Division at pressures of 88.82 ppm,  
134 188.36 ppm, 399.47 ppm, and 528.92 ppm. The accuracy of the measured  $p\text{CO}_2$  data is within 2  
135  $\mu\text{atm}$  (Pierrot et al., 2009). Underway atmospheric  $p\text{CO}_2$  data were simultaneously collected by  
136 the GO system. ~~Due to t~~The biological and physical pumps ~~of carbon cycling~~ in the ocean  
137 (Hardman-Mountford et al., 2009; Bates et al., 1998a, 1998b; Barbini et al., 2003; Sweeney, 2002),  
138 ~~the are the~~ key factors ~~controlling its the variation gradient in sea air in sea surface  $p\text{CO}_2$  levels is~~  
139 ~~the solubility of  $\text{CO}_2$ . In terms of the physical pumps, T~~the solubility of  $\text{CO}_2$  is affected by  
140 temperature and salinity, ~~but the biological pumps, such as, -in the water as well as biological~~  
141 ~~activities, such as~~ phytoplankton, ~~takeing~~ up  $\text{CO}_2$  through photosynthesis ~~and while~~ organisms  
142 ~~releas~~ing  $\text{CO}_2$  ~~it~~ through respiration (Chen et al., 2011). There are several processes that can  
143 influence the distribution of oceanic  $p\text{CO}_2$ .

144 Sea ice melt has a significant impact on the local stratification and circulation in polar regions.  
145 During freezing, brine is rejected from ice, thereby increasing the sea surface salinity. When ice  
146 begins to melt, fresher water is added into the ocean, thereby diluting the ocean water, i.e.,  
147 reducing its salinity. Changes in salinity thus record physical processes. In this study, we treat  
148 salinity as an index for changes in sea ice. The underway SST and conductivity data were recorded  
149 by a Conductivity-Temperature-Depth sensor (CTD, Seabird SBE 21) along the cruise track. Later,  
150 sea surface salinity was calculated based on the recorded conductivity and temperature data. The  
151 distributions of underway SST and SSS are shown in Fig.2c and d.

152 In austral summer, when sea ice started to melt, ice algae were released into the seawater, and  
153 the amount of living biological species and primary productivity increased; thus, high  
154 chlorophyll-a values were observed (Liu et al., 2000; Liu et al., 2003). Previous studies have  
155 reported that the summer sink in the Prydz Bay is biologically driven and that the change in  $p\text{CO}_2$   
156 is often well correlated with the surface chlorophyll-a concentration (Rubin et al., 1998; Gibsonab  
157 et al., 1999; Chen et al., 2011; Xu et al., 2016). The chlorophyll-a value is regarded as an important  
158 controlling factor of  $p\text{CO}_2$ . Remote sensing data of chlorophyll-a obtained from MODIS with a  
159 resolution of 4 km (<http://oceancolor.gsfc.nasa.gov>) were interpolated according to the cruise  
160 track (Fig.2e).

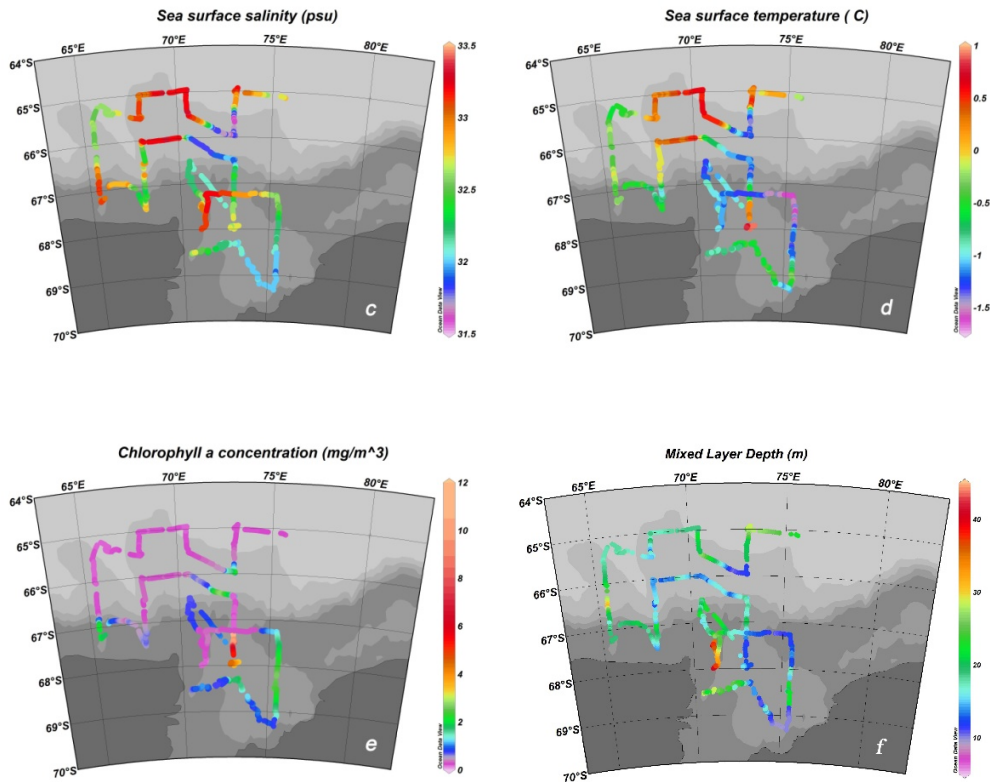
161 The ocean mixed layer is characterized as having nearly uniform physical properties  
162 throughout the layer, with a gradient in its properties occurring at the bottom of the layer. The  
163 mixed layer links the atmosphere to the deep ocean. Previous studies have emphasized the  
164 importance of accounting for vertical mixing through the mixed layer depth (MLD, Dandonneau,  
165 1995; Lüger et al., 2004). The stability and stratification of this layer prevent the upward mixing of  
166 nutrients and limit biological production, thus affecting the sea-air  $\text{CO}_2$  exchange. ~~There are t~~Two  
167 main methods ~~are~~ used to calculate the MLD (Chu and Fan, 2010): one is based on the difference  
168 criterion, and one is based on the gradient criterion. Early studies suggested that the MLD values  
169 determined in the Southern Ocean using the difference criterion are more stable (Brainerd and  
170 Gregg, 1995; Thomson and Fine, 2003). Thus, following Dong et al. (2008), we calculated the  
171 mixed layer depth (see Fig.2f) based on the difference criterion, in which sigma theta changed by  
172  $0.03 \text{ kg/m}^3$ . The MLD values at the stations along the cruise were later gridded linearly to match  
173 the spatial resolution of the underway measurements.

174



175





176  
177

178

179

180

181

## 182 2.2 SOM method and input variables

183

184

185

186

187

188

189

190

191

192

193

194

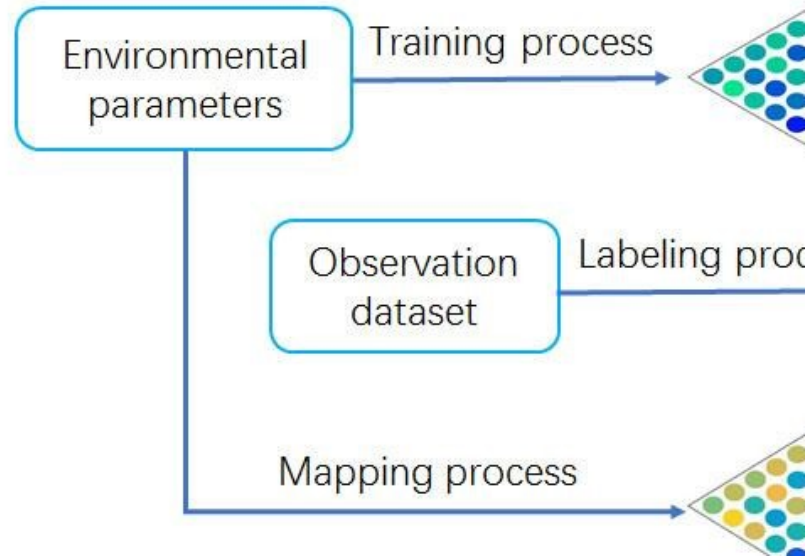
Fig.2 The distributions of underway oceanic and atmospheric  $p\text{CO}_2$ , SST, SSS, and CHL gridded from MODIS, as well as MLD gridded from station surveys, from February to early March.

We hypothesize that oceanic  $p\text{CO}_2$  can be reconstructed using the SOM method with four proxy parameters (Eq. 1): sea surface temperature (SST), chlorophyll-a concentration (CHL), mixed layer depth (MLD), and sea surface salinity (SSS).

$$p\text{CO}_2^{\text{sca}} = \text{SOM}(\text{SST}, \text{CHL}, \text{MLD}, \text{SSS}) \quad (1)$$

The SOM is trained to project the input space of training samples to a feature space (Kohonen, 1984), which is usually represented by grid points in two-dimensional space. Each grid point, which is also called a neuron cell, is associated with a weight vector having the same number of components as the vector of the input data (Zeng et al., 2017). During the SOM analysis, three steps are taken following Nakaoka et al. (2013) to estimate the oceanic  $p\text{CO}_2$  fields (see Fig. 3). Because the four input environmental parameters (SST, CHL, MLD, and SSS) are used to estimate  $p\text{CO}_2$  in this study, each input data set is prepared in 4-D vector form. The input environmental parameters (in this study, SST, CHL, MLD, and SSS) used to estimate  $p\text{CO}_2$  are prepared as a

195 **vector.** Here, the SOM analysis was carried out using the MATLAB SOM tool box 2.0 (Vesanto,  
 196 2002). It has been developed by the Laboratory of Computer and Information Science in the  
 197 Helsinki University of Technology and is available from the following web page:  
 198 <http://www.cis.hut.fi/projects/somtoolbox>.



199  
 200 Fig. 3. Schematic diagram of the main three steps involved in the SOM neural network calculations used to  
 201 obtain weekly  $p\text{CO}_2$  maps for February to early March of 2015.

202 During the training process, each neuron's weight vectors  $(P_i)$ , which are linearly initialized,  
 203 are repeatedly trained by being presented with the input vectors  $(Q_j)$  of environmental parameters  
 204 in the SOM training function. Because SOM analysis is known to be a powerful technique with  
 205 which to estimate  $p\text{CO}_2$  based on the non-linear relationships of the parameters (Telszewski et al.,  
 206 2009), we assumed that the non-linear relationships of the proxy parameters are sufficiently  
 207 represented after the training procedure. During this step, Euclidean distances  $(D)$  are calculated  
 208 between the weight vectors of neurons and the input vectors as shown in Eq.2, and the neuron with  
 209 the shortest distance is selected as the winner. This process results in the clustering of similar  
 210 neurons and the self-organization of the map. The observed oceanic  $p\text{CO}_2$  data are not needed in  
 211 the first step.\_

$$212 \quad \underline{D(P_i, Q_j)} = \sqrt{(P_{i\_SST} - Q_{j\_SST})^2 + (P_{i\_CHL} - Q_{j\_CHL})^2 + (P_{i\_MLD} - Q_{j\_MLD})^2 + (P_{i\_SSS} - Q_{j\_SSS})^2} \dots \text{(Eq. 2)}$$

214 During the second part of the process, each preconditioned SOM neuron is labelled with an  
 215 observation dataset of in situ oceanic  $p\text{CO}_2$  values, and the labelling process technically follows  
 216 the same principles as the training process. The labelling dataset, which consists of the observed  
 217  $p\text{CO}_2$  and normalized SST, CHL, MLD and SSS data, is presented to the neural network. ~~We used~~  
 218 ~~Euclidean distances (i.e., the shortest distances) to select the winner neurons.~~ We calculated the  
 219 D values between trained neurons and observational environmental data sets. The winner neuron is  
 220 selected as in step1 and labelled with an observed  $p\text{CO}_2$  value. After the labelling process, the  
 221 neurons are represented as ~~five-dimensional-5-D~~ 5-D vectors.

222 Finally, during the mapping process, the labelled SOM neurons created by the second process  
 223 and the trained SOM neurons created by the first process are used to produce the oceanic  $p\text{CO}_2$   
 224 value of each winner neuron based on its geographical grid point in the study area.

225 Before the training process, the input training dataset and labelling dataset are analysed and  
 226 prospectively normalized to create an even distribution. The statistics and ranges of the values of  
 227 all variables are presented in Table 1. When the datasets of the four proxy parameters were  
 228 logarithmically normalized, the skewness values of CHL and MLD changed, especially for the  
 229 training dataset. The  $N$  coverage represents the percentage of the training data that are labelled.  
 230 The data  $N$  coverage values of the training data sets of CHL, MLD and SSS are 82.1%, 85% and  
 231 81.1%, respectively, which may be due to their insufficient spatiotemporal coverage and/or bias  
 232 between the labelling and training data sets. The  $N$  coverage of the logarithmic datasets changed to  
 233 93.6% and to 98.7% for CHL and MLD, respectively. Thus, the common logarithms of the CHL  
 234 and MLD values are used for both the training and labelling datasets to resolve the data coverage  
 235 issue arising from significantly increasing the data coverage as well as to overcome the weighting  
 236 issue arising from the different magnitudes between variables (Ultsch and Röske, 2002).

237 Table 1. Statistics of labelling and training data sets showing the distribution and coverage of each  
 238 variable.

Coverage of each variable		SST[C]	CHL[mg/m <sup>3</sup> ]	MLD[m]	SSS[psu]
Labelling	Max	0.81	11.13	40.69	33.81
	Min	-1.44	0.17	7.84	32.43
	Mean	-0.27	3.80	14.41	33.27
	Skewness	0.4(-0.2) <sup>#</sup>	0.8(-0.3)	0.9(0.4)	0.6(0.6)
Training	Max	2.48	40.17	48.95	34.17
	Min	-1.8	0.06	10.46	28.64

Mean	-0.53	1.36	14.79	33.16
Skewness	0.5(-0.6)	4.3(0.5)	2.6(0.8)	-0.9(-1.0)
N coverage* (%)	91.3(92.5) <sup>+</sup>	82.1(93.6)	85.0(98.7)	81.1(80.4)

---

239 # The skewness of the common logarithm of each variable is shown in parentheses.

240 \* [number of training data within the labelling data range]/[total number of training data]

241 + The percent labelling data coverage of normalized variables is shown in parentheses

242 In this study, we construct weekly oceanic  $p\text{CO}_2$  maps from February to early March of  
 243 2015 using four datasets, i.e., SST, CHL, MLD, and SSS. Considering the size of our study  
 244 region, we chose a spatial resolution of  $0.1^\circ$  latitude by  $0.1^\circ$  longitude. For SST, we used daily  
 245 data from AVHRR ONLY (<https://www.ncdc.noaa.gov/oisst>) with a  $1/4^\circ$  spatial resolution (see  
 246 Fig.S1). CHL data represent the 8-D composite chlorophyll-a data from MODIS-Aqua  
 247 (<http://oceancolor.gsfc.nasa.gov>) with a spatial resolution of 4 km (see Fig.S2). We also used the  
 248 daily SSS and MLD data (see Fig.S3-4) from the  $1/12^\circ$  global analysis and forecast product from  
 249 the Copernicus Marine Environment Monitoring Service (CMEMS, <http://marine.copernicus.eu/>).  
 250 Sea ice concentration data are from the daily 3.125-km AMSR2 dataset (Sprenn et al., 2008,  
 251 available on <https://seaice.uni-bremen.de>, see Fig.S5).

252 All daily datasets were first averaged to 8-day fields, which are regarded as weekly in this  
 253 study. The period from the beginning of February to early March comprises four independent  
 254 week series: week-1 (from 02/02/2015 to 02/09/2015), week-2 (from 02/10/2015 to 02/17/2015),  
 255 week-3 (from 02/18/2015 to 02/25/2015), and week-4 (from 02/26/2015 to 03/05/2015). The  
 256 weekly proxy parameters (SCMS) were further re-gridded to a horizontal resolution of  $0.1^\circ \cdot 0.1^\circ$   
 257 using the Kriging method [in SURFER software \(version 7.3.0.35\)](#). In the SOM analyses, input  
 258 vectors with missing elements are excluded. We compared the assimilated datasets of SST from  
 259 AVHRR with the in situ measurements obtained by CTD along the cruise. Their correlation is 0.97,  
 260 and their root-mean-square error (RMSE) is  $0.2^\circ\text{C}$ . Comparing the SSS and MLD fields from the  
 261 Global Forecast system with the in situ measurements yields correlations of 0.76 and 0.74 and  
 262 RMSEs of 0.41 psu and 5.15 m, respectively. The uncertainty of the MODIS CHL data in the  
 263 Southern Ocean is approximately 35% (Xu et al., 2016). For the labelling procedure, the observed  
 264 oceanic  $p\text{CO}_2$  together with the corresponding in situ SST, SSS, MLD, and MODIS CHL products  
 265 in vector form are used as the input dataset.

### 266 2.3 Validation of SOM-derived oceanic $p\text{CO}_2$

267 More realistic  $p\text{CO}_2$  estimates are expected from SOM analyses when the distribution and  
 268 variation ranges of the labelling variables closely reflect those of the training data sets (Nakaoka et  
 269 al., 2013). However, our underway measurements of  $p\text{CO}_2$  values have spatiotemporal limitations  
 270 preventing them from covering the range of variation of the training data sets. To validate the  
 271 oceanic  $p\text{CO}_2$  values reconstructed by the SOM analysis, we used the fugacity of oceanic  $\text{CO}_2$   
 272 datasets from the Surface Ocean  $\text{CO}_2$  Atlas (hereafter referred to as “SOCAT”  
 273 data, <http://www.socat.info>) version 5 database (Bakker et al., 2016). We selected the dataset from  
 274 SOCAT (the EXPCODE is 09AR20150128, see cruise in Fig. 4a) that coincided with the same  
 275 period as our study. The cruise lasted from Feb. 6 to Feb. 27, 2015, and  $f\text{CO}_2$  measurements were  
 276 made every 1 min at a resolution of  $0.01^\circ$ . We recalculated  $p\text{CO}_2$  values based on the obtained  
 277  $f\text{CO}_2$  values provided by the SOCAT data using the fugacity correction (Pfeil et al., 2013).

278

## 279 **2.4 Carbon uptake in the Prydz Bay**

280 The flux of  $\text{CO}_2$  between the atmosphere and the ocean was determined using  $\Delta p\text{CO}_2$  and the  
 281 transfer velocity across the sea-air interface, as shown in Eq. 23, where  $K$  is the gas transfer  
 282 velocity (in  $\text{cm h}^{-1}$ ), and the quadratic relationship between wind speed (in units of  $\text{m s}^{-1}$ ) and the  
 283 Schmidt number is expressed as  $(\text{Sc}/660)^{-0.5}$ .  $L$  is the solubility of  $\text{CO}_2$  in seawater (in  $\text{mol litre}^{-1}$   
 284  $\text{atm}^{-1}$ ) (Weiss, 1974). For the weekly estimation in this study, the scaling factor for the gas transfer  
 285 rate is changed to 0.251 for shorter time scales and intermediate wind speed ranges (Wanninkhof,  
 286 2014). Considering the unit conversion factor (Takahashi et al., 2009), the weekly sea-air carbon  
 287 flux in the Prydz Bay can be estimated using Eq. (34):

$$288 \quad Flux_{\text{sea-air}} = K \times L \times \Delta p\text{CO}_2 \quad (23)$$

$$289 \quad Flux_{\text{sea-air}} [\text{g C}/(\text{m}^2 \cdot \text{week})] = 30.8 \times 10^{-4} \times U^2 \times (p\text{CO}_2^{\text{sea}} - p\text{CO}_2^{\text{air}}) \quad (34)$$

290 where  $U$  represents the wind speed 10 m above sea level, and  $p\text{CO}_2^{\text{sea}}$  and  $p\text{CO}_2^{\text{air}}$  are the partial  
 291 pressures of  $\text{CO}_2$  in sea water and the atmosphere, respectively.

292 We downloaded weekly ASCAT wind speed data (<http://www.remss.com/>, see Fig. S6)  
 293 with a resolution of  $1/4^\circ$  and then gridded the dataset to fit the  $0.1^\circ$  longitude  $\cdot$   $0.1^\circ$  latitude spatial  
 294 resolution of the SOM-derived oceanic  $p\text{CO}_2$ . We gridded the atmospheric  $p\text{CO}_2$  data collected  
 295 along the cruise track to fit the spatial resolution of the SOM-derived oceanic  $p\text{CO}_2$  data using a  
 296 linear method. The total carbon uptake was then obtained by accumulating the flux of each grid in

297 each area according to Jiang et al. (2008) and using the proportion of ice-free areas (Takahashi et  
298 al., 2012). When the ice concentration is less than 10% in a grid, we regard the grid box as  
299 comprising all water. When the ice concentration falls between 10% and 90%, the flux is  
300 computed as being proportional to the water area. In the cases of leads or polynyas due to the  
301 dynamic motion of sea ice (Worby et al., 2008), we assume the grid box to be 10% open water  
302 when the satellite sea ice cover is greater than 90%.

### 303 **3 Results and discussion**

#### 304 **3.1 The distributions of underway measurements**

305 During austral summer, daylight lasts longer and solar radiation increases. With increasing  
306 sea surface temperature, ice shelves break and sea ice melts, resulting in the stratification of the  
307 water column. Starting in the beginning of February, the R/V Xuelong sailed from east to west  
308 along the sea ice edge, and its underway measurements are shown in Fig.2. Based on the water  
309 depth and especially the different ranges of oceanic  $p\text{CO}_2$  (see Fig.2a and Table2), the study area  
310 can be roughly divided into three regions, namely, the Open-ocean region, Sea-ice region and  
311 Shelf region (see Table2).

312 The Open-ocean region ranges northward from 66°S to 64°S, where the Antarctic Divergence  
313 Zone is located and water depths are greater than 3000 m. In the Open-ocean region, the oceanic  
314  $p\text{CO}_2$  was the highest, varying from 291.98  $\mu\text{atm}$  to 379.31  $\mu\text{atm}$ , with a regional mean value of  
315 341.48  $\mu\text{atm}$ . The Antarctic Divergence Zone was characterized by high nutrient concentrations  
316 and low chlorophyll concentrations, with high  $p\text{CO}_2$  attributed to the upwelling of deep waters,  
317 thus suggesting the importance of physical processes in this area (Burkill et al., 1995; Edwards et  
318 al., 2004). The underway sea surface temperatures in this region are relatively high, with an  
319 average value of  $-0.23^\circ\text{C}$  due to the upwelling of Circumpolar Deep Water (CDW), while at the  
320 sea ice edge (73°E, 65.5°S to 72°E, 65.8°S), the SST decreased to less than  $-1^\circ\text{C}$ . From 67.5°E  
321 westward, affected by the large gyre, cold water from high latitudes lowered the SST to less than  
322  $0^\circ\text{C}$ . Near the sea ice edge, SSS decreased quickly to 31.7 psu due to the diluted water; along the  
323 65°S cruise, it reached 33.3 psu; then, moving westward from 67.5°E, affected by the fresher and  
324 colder water brought by the large gyre, it decreased to 32.5 psu. The satellite chlorophyll-a image  
325 showed that the regional mean was as low as  $0.45 \text{ mg/m}^3$ , except when the vessel near the sea ice  
326 edge recorded CHL values that increased to  $2.26 \text{ mg/m}^3$ . The lowest  $p\text{CO}_2$  value was found near  
327 the sea ice edge due to biological uptake. The distribution of MLD varied along the cruise. Near

328 the sea ice edge, because of the melting of ice and direct solar warming, a low-density cap existed  
329 over the water column, and the MLD was as shallow as 10.21 m. The maximum value of MLD in  
330 the Open-ocean region was 31.67 m. In the Open-ocean region, atmospheric  $p\text{CO}_2$  varied from  
331 374.6  $\mu\text{atm}$  to 387.8  $\mu\text{atm}$ . Along the 65°E cruise in the eastern part of the Open-ocean region, the  
332 oceanic  $p\text{CO}_2$  was relatively high, reaching equilibrium with atmospheric  $p\text{CO}_2$ . In the western  
333 part of this region, the oceanic  $p\text{CO}_2$  decreased slightly due to the mixture of low  $p\text{CO}_2$  from  
334 higher latitudes brought by the large gyre. Mixing and upwelling were the dominant factors  
335 affecting the oceanic  $p\text{CO}_2$  in this region.

336 The seasonal Sea-ice region (from 66°S to 67.25°S) is located between the Open-ocean region  
337 and the Shelf region. In this sector, sea ice changed strongly, and the water depth varied sharply  
338 from 700 m to 2000 m. The oceanic  $p\text{CO}_2$  values ranged from 190.46  $\mu\text{atm}$  to 364.43  $\mu\text{atm}$ , with a  
339 regional mean value of 276.48  $\mu\text{atm}$ . Sea ice continued to change and reform from late February to  
340 the beginning of March (Fig. 6). The regional mean sea surface temperature decreased slightly  
341 compared to that in the Open-ocean region, and the average value was -0.72°C. With the rapid  
342 changes in sea ice, the sea surface temperature and salinity varied sharply from -1.3°C to 0.5°C  
343 and from 31.8 psu to 33.3 psu, respectively. When sea ice melted, the water temperature increased,  
344 biological activity increased, and the chlorophyll-a value increased slightly to reach a regional  
345 average of 0.59 mg/m<sup>3</sup>. Due to the rapid change in sea ice cover, the value of MLD varied from  
346 12.8 m to 30.9 m.

347 The Shelf region (from 67.25°S southward) is characterized by shallow depths of less than  
348 700 m, and it is surrounded by the Amery Ice Shelf and the West Ice Shelf. Water inside the Shelf  
349 region is formed by the modification of low-temperature and high-salinity shelf water (Smith et al.,  
350 1984). The Prydz Bay coastal current flows from east to west in the semi-closed bay. The oceanic  
351  $p\text{CO}_2$  values in this region were the lowest of those in all three sectors; these values ranged from  
352 151.70  $\mu\text{atm}$  to 277.78  $\mu\text{atm}$ , with a regional average of 198.72  $\mu\text{atm}$ . A fresher, warmer surface  
353 layer is always present over the bay, which is known as the Antarctic Surface Water (ASW).  
354 During our study period, the Shelf region was the least ice-covered region. A large volume of  
355 freshwater was released into the bay, resulting in low sea surface temperature (an average of  
356 -0.61°C) and salinity (an average of 32.4 psu) values. As shown in Fig.2f, the mixed layer depth in  
357 most of the inner shelf is low. Due to the vast shrinking of sea ice and strong stratification in the  
358 upper water, algal blooming occurred and chlorophyll values were high, with an average of 1.93

359 mg/m<sup>3</sup>. The chlorophyll-a value was remarkably high, reaching 11.04 mg/m<sup>3</sup> when sea ice retreated  
 360 eastwardly from 72.3°E, 67.3°S to 72.7°E, 68°S. The biological pump became the dominant  
 361 factor controlling the distribution of oceanic *p*CO<sub>2</sub>. In the bay mouth close to the Fram Bank, due  
 362 to local upwelling, the water salinity increased remarkably to approximately 33.2 psu.

363 Table 2 The regional mean values of underway measurements in three sub-regions

	<i>p</i> CO <sub>2</sub> [μatm]	SST [° ]	CHL [mg/m <sup>3</sup> ]	MLD [m]	SSS [psu]
Open-ocean region (66°S - 64°S)	341.48	-0.23	0.45	20.13	32.61
Sea-ice region (66°S - 67.25°S)	276.48	-0.72	0.59	19.44	32.42
Shelf region (67.25°S - 70°S)	198.72	-0.61	1.95	16.84	32.46

364

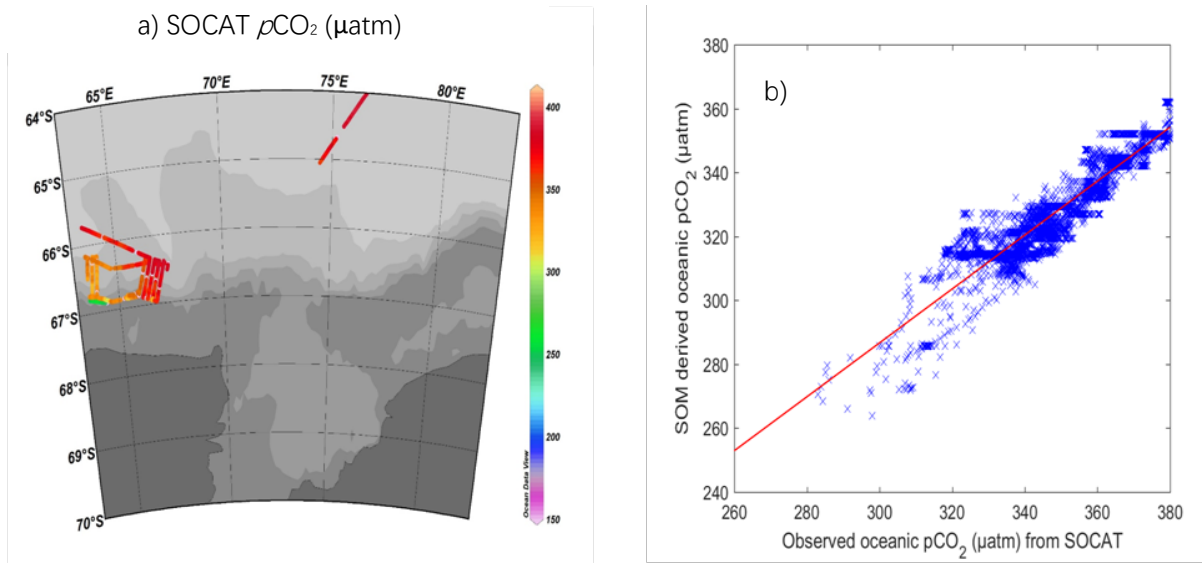
### 365 3.2 Quality and maps of SOM-derived oceanic *p*CO<sub>2</sub>

366 We selected SOM-derived oceanic *p*CO<sub>2</sub> values to fit the cruise track of SOCAT for the same  
 367 period in February 2015 using a nearest-grid method. The RMSE between the SOCAT data and  
 368 the SOM-derived result was calculated as follows:

$$369 \quad RMSE = \sqrt{\frac{\sum (pCO_2^{sea}(SOM) - pCO_2^{sea}(SOCAT))^2}{n}} \quad (4)$$

370 where *n* is the number of validation datasets. The RMSE can be interpreted as an estimation of the  
 371 uncertainty in the SOM-derived oceanic *p*CO<sub>2</sub> in the Prydz Bay. In this study, the RMSE of the  
 372 SOM-derived oceanic *p*CO<sub>2</sub> and SOCAT datasets is 22.14 μatm, and the correlation coefficient  
 373 R<sup>2</sup> is 0.82. The absolute mean difference is 23.58 μatm. The RMSE obtained in our study is  
 374 consistent with the accuracies (6.9 μatm to 24.9 μatm) obtained in previous studies that used  
 375 neuron methods to reconstruct oceanic *p*CO<sub>2</sub> (Nakaoka et al., 2013; Zeng et al., 2002; Sarma et al.,  
 376 2006; Jo Y H et al., 2012; Hales et al., 2012; Telszewshi et al., 2009). The precision of this study is  
 377 on the high side of those that have been previously reported. The slope of the scatter plot  
 378 indicates that the SOM-derived oceanic *p*CO<sub>2</sub> data are lower than the SOCAT data (see Fig. 4b).  
 379 Thus, the precision of these data may have greater uncertainty because the SOCAT dataset does  
 380 not cover the low-*p*CO<sub>2</sub> area towards the south. Thus, increasing the spatial coverage of the  
 381 labelling data will help increase the precision of the SOM-derived oceanic *p*CO<sub>2</sub>.





382 Fig. 4 a) The cruise lines from SOCAT used to validate the SOM-derived oceanic  $p\text{CO}_2$  for the study period in  
 383 2015; b) comparison between the SOM-derived and observed SOCAT oceanic  $p\text{CO}_2$  data.

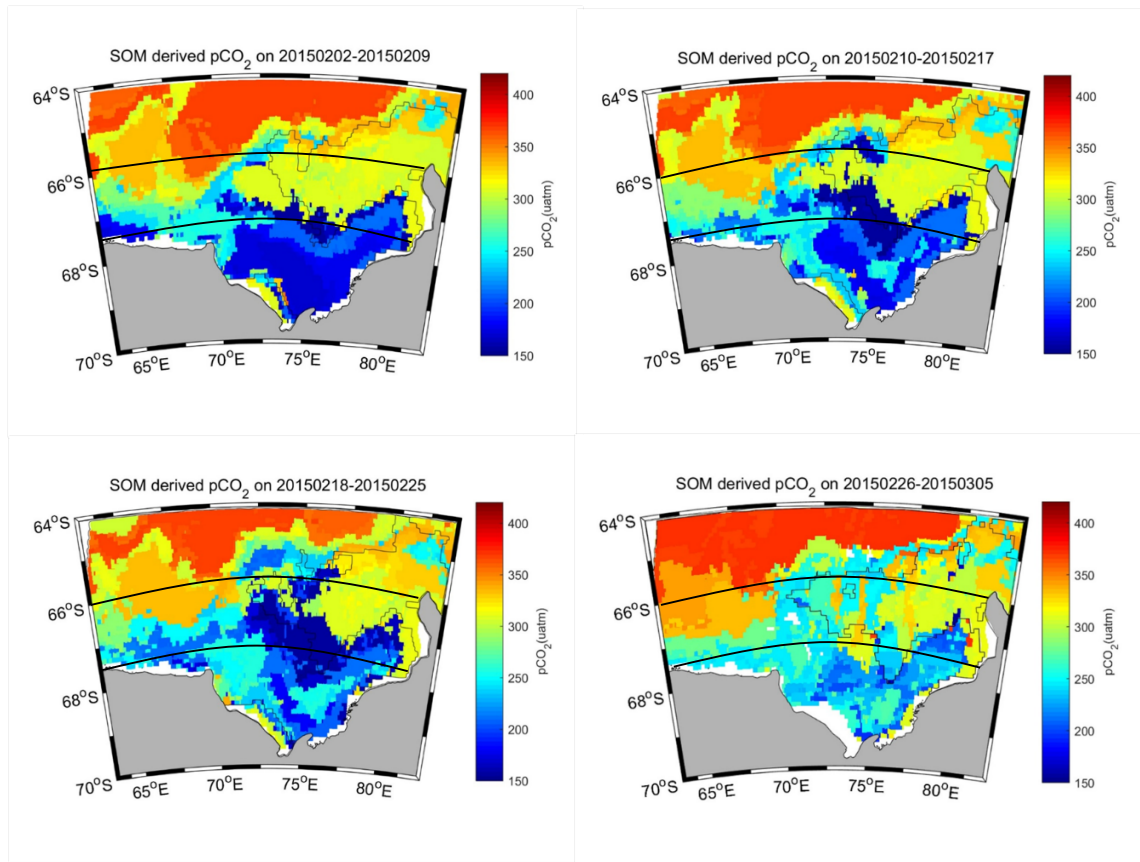
384

### 385 3.3 Spatial and temporal distributions of SOM-derived oceanic $p\text{CO}_2$

386 The weekly mean maps of SOM-derived oceanic  $p\text{CO}_2$  in the Prydz Bay are shown in Fig. 5.  
 387 In the Open-ocean region, the oceanic  $p\text{CO}_2$  values were higher than those in the other two  
 388 regions due to the upwelling of the CDW. During all four weeks, this region was nearly ice-free,  
 389 while the average sea ice coverage was 18.14% due to the presence of permanent sea ice (see  
 390 Fig.6). The oceanic  $p\text{CO}_2$  distribution decreased from east to west in the Open-ocean region,  
 391 with lower values observed at the edge of sea ice. In the western part of the Open-ocean region,  
 392 oceanic  $p\text{CO}_2$  decreased due to mixing with low oceanic  $p\text{CO}_2$  flowing from high-latitude regions  
 393 caused by the large gyre. From week-1 to week-4, the maximum oceanic  $p\text{CO}_2$  increased slightly  
 394 and reached 381.42  $\mu\text{atm}$ , which was equivalent to the  $p\text{CO}_2$  value of the atmosphere.

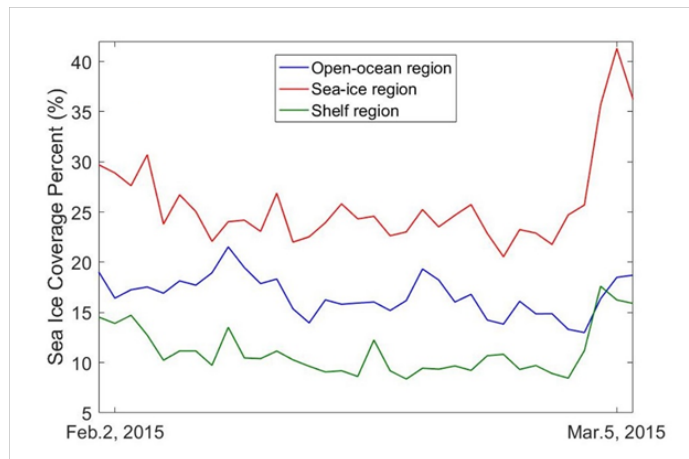
395 In the Sea-ice region, sea ice continued to rapidly melt and reform. The weekly mean sea ice  
 396 coverage percentage was 29.54%, occupying nearly one-third of the Sea-ice region. As shown in  
 397 Fig.5, the gradient of the oceanic  $p\text{CO}_2$  distribution increased from south to north affected by the  
 398 flow coming from the Shelf region by the large gyre. In the eastern part of this region, adjacent  
 399 to the sea ice edge, the oceanic  $p\text{CO}_2$  values were lower. The oceanic  $p\text{CO}_2$  changed sharply from  
 400 155.86  $\mu\text{atm}$  (near the sea ice edge) to 365.11  $\mu\text{atm}$  (close to the Open-ocean region).

401 In austral winter, the entire Prydz Bay basin is fully covered by sea ice, except in a few areas,  
402 i.e., the polynyas, which remain open due to katabatic winds (Liu et al., 2017). When the austral  
403 summer starts, due to coincident high wind speeds, monthly peak tides, and/or the effect of  
404 penetrating ocean swells, the sea ice in the Shelf region starts to melt first in early summer (Lei et  
405 al., 2010), forming the Prydz Bay Polynya. The semi-closed polynya functions as a barrier for  
406 water exchange in the Shelf region and causes a lack of significant bottom water production,  
407 hindering the outflow of continental shelf water and the inflow of Antarctic circle deep water,  
408 resulting in the longer residence time of vast melting water and enhanced stratification (Sun et al.,  
409 2013). Due to vast melting of the sea ice, the sea surface salinity decreased and algae bloomed;  
410 biological productivity promptly increased, and the chlorophyll-a concentration reached its peak  
411 value. As shown in Fig. 5, the distribution of oceanic  $p\text{CO}_2$  in the Shelf region was characterized  
412 by its lowest values. The obvious drawdown of oceanic  $p\text{CO}_2$  occurred in the Shelf region due to  
413 phytoplankton photosynthesis during this summer bloom. The lowest oceanic  $p\text{CO}_2$  in the Shelf  
414 region was  $153.83 \mu\text{atm}$ , except at the edge of the West Ice Shelf, where the Shelf oceanic  $p\text{CO}_2$   
415 exceeded  $300 \mu\text{atm}$ . The oceanic  $p\text{CO}_2$  was the lowest in week-1, which coincided with a peak in  
416 chlorophyll-a, as evidenced by satellite images. The regional oceanic  $p\text{CO}_2$  increased slightly in  
417 week-4 compared to the other three weeks.



418

419 Fig.5 Distribution of weekly mean SOM-derived oceanic  $p\text{CO}_2$  in the Prydz Bay (unit:  $\mu\text{atm}$ ) from Feb. 2,  
 420 2015 to Mar. 5, 2015. The black contour represents a sea ice concentration of 15%.



421

422 Fig. 6 Percentage of sea ice coverage in three sub-regions from Feb. 2, 2015 to Mar. 5, 2015 (blue:  
 423 Open-ocean region; red: Sea-ice region; green: Shelf region).

424 **3.4 Carbon uptake in the Prydz Bay**

425 During our study period, the entire region was undersaturated, with CO<sub>2</sub> being absorbed  
426 by the ocean. The regional averaged ocean-air  $p\text{CO}_2$  difference ( $\Delta p\text{CO}_2$ ) was highest in the Shelf  
427 region, followed by the Sea-ice region and Open-ocean region (see Table3). The regional and  
428 weekly mean  $\Delta p\text{CO}_2$  in the Shelf region changed from -184.31  $\mu\text{atm}$  in week-1 to -141.00  $\mu\text{atm}$  in  
429 week-2 as chlorophyll decreased. The  $\Delta p\text{CO}_2$  in the Sea-ice region and Open-ocean region  
430 showed the same patterns, increasing from week-1 to week-3 and then decreasing in week-4.  
431 Based on the  $\Delta p\text{CO}_2$  and wind speed data, the uptake of CO<sub>2</sub> in these three regions is presented in  
432 Table3. The uncertainty of the carbon uptake depends on the errors associated with the wind speed,  
433 the scaling factor and the accuracy of the SOM-derived  $p\text{CO}_2$  according to Eq.34. The scaling  
434 factor will yield a 20% uncertainty in the regional flux estimation. The errors in the wind speeds of  
435 the ASCAT dataset are assumed to be 6% (Xu et al., 2016); the error in the quadratic wind speed is  
436 12%. The RMSE of the SOM-derived  $p\text{CO}_2$  is 22.14  $\mu\text{atm}$ . Considering the errors described above  
437 and the uncertainty occurring when the sea-air computation expression is simplified (1.39%, Xu et  
438 al., 2016), the total uncertainty of the final uptake is 27%. In the Shelf region, the low oceanic  
439  $p\text{CO}_2$  levels drove relatively intensive CO<sub>2</sub> uptake from the atmosphere. The carbon uptake in the  
440 Shelf region changed ~~mildly~~ from week-1 ( $2.51 \pm 0.68 \text{ TgC}$ ,  $10^{12} \text{ gram} = \text{Tg}$ ) to week-2  
441 ( $2.77 \pm 0.75 \text{ TgC}$ ). In contrast, in week-3, the wind speed slowed down, resulting in the uptake of  
442 CO<sub>2</sub> in the Shelf region decreasing to  $2.10 \pm 0.57 \text{ TgC}$ . In week-4, even though the  $\Delta p\text{CO}_2$  was the  
443 lowest of all four weeks, the total absorption still increased to  $2.63 \pm 0.715 \text{ TgC}$  due to the high  
444 wind speed (with an average value of 7.92 m/s). The total carbon uptake in the three regions of the  
445 Prydz Bay, integrated from February to early March of 2015, was 23.57 TgC, with an uncertainty  
446 of  $\pm 6.36 \text{ TgC}$ .

447 Table3 Regional and weekly mean  $\Delta p\text{CO}_2$ , wind speed and uptake of CO<sub>2</sub> in three  
448 sub-regions (negative values represent directions moving from air to sea).

		Week-1	Week-2	Week-3	Week-4	Uptake in 4 weeks [Tg]
Open-ocean region (66°S - 64°S)	$\Delta p\text{CO}_2$ [ $\mu\text{atm}$ ]	-34.11	-42.69	-51.94	-34.08	
	Wind speed [m/s]	7.82	8.54	7.02	9.31	-5.74
	Uptake [Tg]	-1.08	-1.55	-1.51	-1.60	
Sea-ice region (66°S - 67.25°S)	$\Delta p\text{CO}_2$ [ $\mu\text{atm}$ ]	-115.92	-119.83	-127.74	-86.72	
	Wind speed [m/s]	7.67	8.17	6.39	8.36	-7.82
	Uptake [Tg]	-2.11	-2.35	-1.73	-1.63	
Shelf region (67.25°S - 70°S)	$\Delta p\text{CO}_2$ [ $\mu\text{atm}$ ]	-184.32	-170.23	-158.61	-141.03	
	Wind speed [m/s]	6.92	7.27	6.67	7.92	-10.01
	Uptake [Tg]	-2.51	-2.77	-2.10	-2.63	

449

450 Roden et al. (2013) estimated the coastal Prydz Bay to be an annual net sink for CO<sub>2</sub> of  
451 0.54±0.11 mol/(m<sup>2</sup>·year), i.e., 1.48±0.3 g/(m<sup>2</sup>·week). Gibsonab et al. (1999) estimated the average  
452 sea-air flux in the summer ice-free period to be more than 30 mmol/(m<sup>2</sup>·day), i.e., 9.2 g/(m<sup>2</sup>·week).  
453 Our study suggests that the sea-air flux during the strongest period of the year, i.e., February, could  
454 be much larger. The average flux obtained here, 18.84 g/(m<sup>2</sup>·week), is twice as large as the average  
455 value estimated over a longer period (November to February) reported by Gibsonab et al. (1999).

456 As the region recording the strongest surface unsaturation of these three regions in summer,  
457 the Shelf region has a potential carbon uptake of 10.01±2.7 Tg C from February to early March,  
458 which accounts for approximately 5.0‰-6.7‰ of the net global ocean CO<sub>2</sub> uptake according to  
459 Takahashi et al. (2009), even though its total area is only 78\*10<sup>3</sup> km<sup>2</sup>. Due to the sill constraint,  
460 there is limited exchange between water masses in and outside the Prydz Bay. During winter, the  
461 dense water formed by the ejection of brine in the Bay can potentially uptake more anthropogenic  
462 CO<sub>2</sub> from the atmosphere that can descend to greater depths, thus enhancing the acidification in  
463 deep water. According to Shadwick et al. (2013), the winter values of *p*H and Ω decrease more  
464 remarkably than those in summer. As the bottom water in the Prydz Bay is a possible source of  
465 Antarctic Bottom Water (Yabuki et al., 2006), the Shelf region may transfer anthropogenic CO<sub>2</sub> at  
466 the surface to deep water and may thus influence the acidification of the deep ocean over long  
467 timescales.

468

#### 469 **4 Summary**

470 Based on the different observed ranges of the distribution of ocean *p*CO<sub>2</sub>, the Prydz Bay  
471 region was divided into three sectors from February to early March of 2015. In the Shelf region,  
472 biological factors exerted the main control on oceanic *p*CO<sub>2</sub>, while in the Open-ocean region,  
473 mixing and upwelling were the main controls. In the Sea-ice region, due to rapid changes in sea ice,  
474 oceanic *p*CO<sub>2</sub> was controlled by both biological and physical processes. SOM is an important tool  
475 for the quantitative assessment of oceanic *p*CO<sub>2</sub> and its subsequent sea-air carbon flux, especially  
476 in dynamic, high-latitude, and seasonally ice-covered regions. The estimated results revealed that  
477 the SOM technique ~~can~~ be used to reconstruct the variations in oceanic *p*CO<sub>2</sub> associated with  
478 biogeochemical processes expressed by the variability in four proxy parameters: SST, CHL, MLD  
479 and SSS. The RMSE of the SOM-derived oceanic *p*CO<sub>2</sub> is 22.14 μatm for the SOCAT dataset.

480 From February to early March of 2015, the Prydz Bay region was a strong carbon sink, with a  
481 carbon uptake of  $23.57 \pm 6.36$  TgC. The strong potential uptake of anthropogenic CO<sub>2</sub> in the Shelf  
482 region will enhance the acidification in the deep water region of the Prydz Bay and may thus  
483 influence the acidification of the deep ocean in the long run because it contributes to the formation  
484 of Antarctic Bottom Water.

#### 485 **Acknowledgments**

486 This work is supported by National Natural Science Foundation of China  
487 (NSFC41506209, 41630969, 41476172, 41230529), Qingdao National Laboratory for marine  
488 science and technology (QNL2016ORP0109), Chinese Projects for Investigations and  
489 Assessments of the Arctic and Antarctic (CHINARE2012-2020 for 01-04, 02-01, and 03-04). This  
490 work is also supported by Korea Polar Research Institute grants PE18060 and PE18070. We would  
491 like to thank China Scholarship Council (201704180019) and State Administration of Foreign  
492 Experts Affairs P. R. China for their support in this research. We would like to thank the carbon  
493 group led by Zhongyong Gao and Heng Sun in GCMAC and the crew on R/V Xuelong for their  
494 support on the cruise. We are thankful to contributors of the SOCAT database for validated *p*CO<sub>2</sub>  
495 data and Mercator Ocean for providing the Global Forecast model output. We deeply appreciate  
496 Dr. Xianmin Hu in Bedford Institute of Oceanography, who provided us with useful technical  
497 instructions.

#### 498 **References**

- 499
- 500 1. Bakker, D. C. E., Pfeil, B. Landa, C. S., Metzl, N., O'Brien, K. M., Olsen, A., Smith, K.,  
501 Cosca, C., Harasawa, S., Jones, S. D., Nakaoka, S., Nojiri, Y., Schuster, U., Steinhoff, T.,  
502 Sweeney, C., Takahashi, T., Tilbrook, B., Wada, C., Wanninkhof, R., Alin, S. R., Balestrini,  
503 C. F., Barbero, L., Bates, N. R., Bianchi, A. A., Bonou, F., Boutin, J., Bozec, Y., Burger, E.  
504 F., Cai, W.-J., Castle, R. D., Chen, L., Chierici, M., Currie, K., Evans, W., Featherstone, C.,  
505 Feely, R. A., Fransson, A., Goyet, C., Greenwood, N., Gregor, L., Hankin, S.,  
506 Hardman-Mountford, N. J., Harlay, J., Hauck, J., Hoppema, M., Humphreys, M. P., Hunt, C.  
507 W., Huss, B., Ibáñez, J. S. P., Johannessen, T., Keeling, R., Kitidis, V., Körtzinger, A.,  
508 Kozyr, A., Krasakopoulou, E., Kuwata, A., Landschützer, 3P., Lauvset, S. K., Lefèvre, N.,  
509 Lo Monaco, C., Manke, A., Mathis, J. T., Merlivat, L., Millero, F. J., Monteiro, P. M. S.,  
510 Munro, D. R., Murata, A., Newberger, T., Omar, A. M., Ono, T., Paterson, K., Pearce, D.,

- 511 Pierrot, D., Robbins, L. L., Saito, S., Salisbury, J., Schlitzer, R., Schneider, B., Schweitzer,  
512 R., Sieger, R., Skjelvan, I., Sullivan, K. F., Sutherland, S. C., Sutton, A. J., Tadokoro, K.,  
513 Telszewski, M., Tuma, M., Van Heuven, S. M. A. C., Vandemark, D., Ward, B., Watson, A.  
514 J., and Xu, S.: A multi-decade record of high quality  $f\text{CO}_2$  data in version 3 of the Surface  
515 Ocean  $\text{CO}_2$  Atlas (SOCAT). *Earth System Science Data* 8:  
516 383-413.doi:10.5194/essd-8-383-2016, 2016.
- 517 2. Barbini, R., Fantoni, R., Palucci, A., Colao, F., Sandrini, S., Ceradini, S., Tositti, L.,  
518 Tubertini, O., and Ferrari, G. M.: Simultaneous measurements of remote lidar chlorophyll  
519 and surface  $\text{CO}_2$  distributions in the Ross Sea. *International Journal of Remote Sensing*, 24,  
520 3807-3819, 2003.
- 521 3. Bates, N. R., Hansell, D. A., Carlson, C. A., and Gordon, L. I.: Distribution of  $\text{CO}_2$  species,  
522 estimates of net community production, and air–sea  $\text{CO}_2$  exchange in the Ross Sea polynya,  
523 *Journal of Geophysical Research*, 103, 2883-2896, 1998a.
- 524 4. Bates, N. R., Takahashi, T., Chipman, D. W., and Knapp, A. H.: Variability of  $p\text{CO}_2$  on diel  
525 to seasonal time scales in the Sargasso Sea, *Journal of Geophysical Research*, 103,  
526 15567-15585, 1998b.
- 527 5. Brainerd, K. E., and Gregg, M. C.: Surface mixed and mixing layer depth, *Deep Sea Res.*,  
528 part A, 42, 1521-1543, 1995.
- 529 6. Burkill, P. H., Edwards, E. S., and Sleight, M. A.: Microzooplankton and their role in  
530 controlling phytoplankton growth in the marginal ice zone of the Bellingshausen Sea, *Deep*  
531 *Sea Research Part II: Topical Studies in Oceanography*, 42(4), 1277-1290, 1995.
- 532 7. Chen, L., Xu, S., Gao, Z., Chen, H., Zhang, Y., Zhan, J., and Li, W.: Estimation of monthly  
533 air-sea  $\text{CO}_2$  flux in the southern Atlantic and Indian Ocean using in-situ and remotely sensed  
534 data, *Remote Sensing of Environment*, 115(8), 1935-1941, 2011.
- 535 8. Chierici, M., Olsen, A., Johannessen, T., Trinanes, J., and Wanninkhof, R.: Algorithms to  
536 estimate the carbon dioxide uptake in the northern North Atlantic using ship-observations,  
537 satellite and ocean analysis data, *Deep-Sea Res. Pt. II*, 56(8-10), 630-639, 2009.
- 538 9. Chu, P. C., and Fan, C.: Optimal linear fitting for objective determination of ocean mixed  
539 layer depth from glider profiles, *Journal of Atmospheric and Oceanic Technology*, 27(11):  
540 1893-1989, 2010.
- 541 10. Dandonneau, Y.: Sea-surface partial pressure of carbon dioxide in the eastern equatorial

- 542 Pacific (August 1991 to October 1992): A multivariate analysis of physical and biological  
543 factors, *Deep Sea Research II*, 42(2-3), 349-364, 1995.
- 544 11. Dong, S., Sprintall, J., Gille, S. T., and Talley, L.: Southern Ocean mixed-layer depth from  
545 Argo float profiles, *Journal of Geophysical Research*, 113, C06013, doi:  
546 10.1029/2006JC004051, 2008.
- 547 12. Edwards, A. M., Platt, T., and Sathyendranath, S.: The high-nutrient, low-chlorophyll  
548 regime of the ocean: limits on biomass and nitrate before and after iron enrichment,  
549 *Ecological Modelling*, 171, 103-125, 2004.
- 550 13. Friedrich, T., and Oschlies, A.: Basin-scale  $p\text{CO}_2$  maps estimated from ARGO float data: A  
551 model study, *J. Geophys. Res.*, 114, C10012, doi:10.1029/2009JC005322, 2009b.
- 552 14. Friedrich, T., and Oschlies, A.: Neural network-based estimates of North Atlantic surface  
553  $p\text{CO}_2$  from satellite data: A methodological study, *J. Geophys. Res.*, 114, C03020,  
554 doi:10.1029/2007JC004646, 2009a.
- 555 15. Gao, Z., Chen, L., and Gao, Y.: Air-sea carbon fluxes and their controlling factors in the  
556 Prydz Bay in the Antarctic, *Acta Oceanologica Sinica*, 3(27), 136-146, 2008.
- 557 16. Gibson, P. B., Perkins-Kirkpatrick, S. E., Uotila, P., Pepler, A. S., and Alexander, L. V.: On  
558 the use of self-organizing maps for studying climate extremes, *Journal of Geophysical*  
559 *Research: Atmospheres*, 122, 3891-3903, 2017.
- 560 17. Gibson, J. A.E., and Trull, T. W.: Annual cycle of  $f\text{CO}_2$  under sea-ice and in open  
561 water in Prydz Bay, east Antarctica, *Marine Chemistry*, Volume 66, Issues 3-4, 187-200,  
562 1999.
- 563 18. Hales, B., Strutton, P., Saraceno, M., Letelier, R., Takahashi, T., Feely, R., Sabine, C., and  
564 Chavez, F.: Satellite-based prediction of  $p\text{CO}_2$  in coastal waters of the eastern North Pacific,  
565 *Progress in Oceanography*, 103, 1-15, 2012.
- 566 19. Hardman-Mountford, N., Litt, E., Mangi, S., Dye, S., Schuster, U., Bakker, D., and Watson,  
567 A.: Ocean uptake of carbon dioxide ( $\text{CO}_2$ ), MCCIP BriefingNoteswww.mccip.org.uk, 9pp,  
568 2009.
- 569 20. Heil, P., Allison, I. and Lytle, V. I.: Seasonal and interannual variations of the oceanic heat  
570 flux under a landfast Antarctic sea ice cover, *J. Geophys. Res.*, 101(C11), 25,741-25,752,  
571 doi: 10.1029/96JC01921, 1996.
- 572 21. Huang, J., Xu, F., Zhou, K., Xiu, P., and Lin, Y.: Temporal evolution of near-surface



- 573 chlorophyll over cyclonic eddy lifecycles in the southeastern Pacific, *Journal of Geophysical*  
574 *Research: Oceans* 122, 6165-6179, 2017a.
- 575 22. Huang, W., Chen, R., Yang, Z., Wang, B., and Ma, W.: Exploring the combined effects of  
576 the Arctic Oscillation and ENSO on the wintertime climate over East Asia using  
577 self-organizing maps, *Journal of Geophysical Research: Atmospheres*, 122, 9107-9129,  
578 2017b.
- 579 23. Iskandar, I.: Seasonal and interannual patterns of sea surface temperature in Banda Sea as  
580 revealed by self-organizing map, *Continental Shelf Research*, 30, 1136-1148, 2010.
- 581 24. Jacobs, S. S. and Georgi, D. T.: Observations on the south-west Indian/Antarctic Ocean, In  
582 *A Voyage of Discovery*, ed. by M. Angel, *Deep-Sea Res.*, 24(suppl.), 43-84, 1977.
- 583 25. Jamet, C., Moulin, C., and Lefèvre, N.: Estimation of the oceanic  $p\text{CO}_2$  in the North Atlantic  
584 from VOS lines in situ measurements: Parameters needed to generate seasonally mean maps,  
585 *Ann. Geophys.*, 25, 2247-2257, 2007, <http://www.ann-geophys.net/25/2247/2007/>.
- 586 26. Jiang, L. Q., Cai, W. J., Wanninkhof, R., Wang, Y., and Lüger, H.: Air-sea  $\text{CO}_2$  fluxes on  
587 the U.S. South Atlantic Bight: Spatial and seasonal variability, *Journal of Geophysical*  
588 *Research*, 113 (2008), C07019, doi:10.1029/2007JC004366, 2008.
- 589 27. Jo, Y. H., Dai, M. H., Zhai, W. D., Yan, X. H., and Shang, S. L.: On the variations of sea  
590 surface  $p\text{CO}_2$  in the northern South China sea: A remote sensing based neural network  
591 approach, *Journal of Geophysical Research*, 117, C08022, doi:10.1029/2011JC007745,  
592 2012.
- 593 28. Kohonen, T.: *Self-Organization and Associative Memory*, Springer, Berlin, 1984.
- 594 29. Lafevre, N., Watson, A. J., and Watson, A. R.: A comparison of multiple regression and  
595 neural network techniques for mapping in situ  $p\text{CO}_2$  data, *Tellus B*, 57(5), 375-384, 2005.
- 596 30. Laruelle, G. G., Landschützer, P., Gruber, N., Tison, J. L., Delille, B., and Regnier, P.:  
597 Global high resolution monthly  $p\text{CO}_2$  climatology for the coastal ocean derived from neural  
598 network interpolation, *Biogeosciences*, 14, 4545-4561, 2017.
- 599 31. Lei, R., Li, Z., Cheng, B., Zhang, Z., and Heil, P.: Annual cycle of landfast sea ice in Prydz  
600 Bay, East Antarctica, *Journal of Geophysical Research Atmospheres*, 115(C2), C02006,  
601 doi:10.1029/2008JC005223, 2010.
- 602 32. Liu C., Wang Z., Cheng C., Xia R., Li B., and Xie Z.: Modeling modified circumpolar deep  
603 water intrusions onto the Prydz Bay continental shelf, East Antarctica, *Journal of*

- 604 Geophysical Research, Vol. 122, Issue 7, 5198-5217. DOI: 10.1002/2016JC012336, 2017.
- 605 33. Liu, Y., Weisberg, R. H., and He, R.: Sea Surface Temperature Patterns on the West Florida  
606 Shelf Using Growing Hierarchical Self-Organizing Maps, *Journal of Atmospheric and*  
607 *Oceanic Technology*, 23, 325-338, 2006.
- 608 34. Liu, Z. L., Ning, X. R., Cai, Y. M., Liu, C. G., and Zhu, G. H.: Primary productivity and  
609 chlorophyll a in the surface water on the route encircling the Antarctica during austral  
610 summer of 1999/2000, *Polar Research*, 112(4), 235-244, 2000.
- 611 35. Liu, Z., and Cheng Z.: The distribution feature of size-fractionated chlorophyll a and  
612 primary productivity in Prydz Bay and its north sea area during the austral summer, *Chinese*  
613 *Journal of Polar Science*, 14(2): 81-89, 2003.
- 614 36. Lüger, H., Wallace, D. W. R., Körtzinger, A., and Nojiri, Y.: The  $p\text{CO}_2$  variability in the  
615 midlatitude North Atlantic Ocean during a full annual cycle, *Global Biogeochem. Cycles*,  
616 18, GB3023, doi:10.1029/2003GB002200, 2004.
- 617 37. Metzl, N., Brunet, C., Jabaud-Jan, A., Poisson, A., and Schauer, B.: Sumer and winter  
618 air-sea  $\text{CO}_2$  fluxes in the Southern Ocean, *Deep-Sea Research*, 153: 1548-1563, 2006.
- 619 38. Middleton, J. H., and Humphries, S. E.: Thermohaline structure and mixing in the region of  
620 Prydz Bay, Antarctica, *Deep Sea Research Part A, Oceanographic Research Papers*, 36(8),  
621 1255-1266, 1989.
- 622 39. Morrison, J. M., Gaurin, S., Codispoti, L. A., Takahashi, T., Millero, F. J., Gardner, W. D.,  
623 and Richardson, M. J.: Seasonal evolution of hydrographic properties in the Antarctic  
624 circumpolar current at 170W during 1997-1998, *Deep-Sea Research*, 148: 3943-3972, 2001.
- 625 40. Nakaoka, S., Telszewski, M., Nojiri, Y., Yasunaka, S., Miyazaki, C., Mukai, H., and Usui,  
626 N.: Estimating temporal and spatial variation of ocean surface  $p\text{CO}_2$  in the North Pacific  
627 using a self-organizing map neural network technique, *Biogeosciences*, 10, 6093-6106,  
628 2013.
- 629 41. Nunes Vaz, R. A., and Lennon, G. W.: Physical oceanography of the Prydz Bay region of  
630 Antarctic waters, *Deep Sea Research Part I: Oceanography Research Papers*, 43(5), 603-641,  
631 1996.
- 632 42. Olsen, A., Trinanes, J. A., and Wanninkhof, R.: Sea-air flux of  $\text{CO}_2$  in the Caribbean Sea  
633 estimated using in situ and remote sensing data, *Remote Sens. Environ.*, 89, 309-325, 2004.
- 634 43. Pfeil, B., Olsen, A., Bakker, D. C. E., Hankin, S., Koyuk, H., Kozyr, A., Malczyk, J.,

635 Manke, A., Metzl, N., Sabine, C. L., Akl, J., Alin, S. R., Bellerby, R. G. J., Borges, A.,  
636 Boutin, J., Brown, P. J., Cai, W.-J., Chavez, F. P., Chen, A., Cosca, C., Fassbender, A. J.,  
637 Feely, R. A., González-Dávila, M., Goyet, C., Hardman- Mountford, N., Heinze, C., Hood,  
638 M., Hoppema, M., Hunt, C. W., Hydes, D., Ishii, M., Johannessen, T., Jones, S. D., Key, R.  
639 M., Körtzinger, A., Landschützer, P., Lauvset, S. K., Lefèvre, N., Lenton, A., Lourantou, A.,  
640 Merlivat, L., Iidorikawa, T., Mintrop, L., Miyazaki, C., Murata, A., Nakadate, A., Nakano,  
641 Y., Nakaoka, Y. Nojiri, A. M. Omar, X. A. Padin, G.-H. Park, K. Paterson, F. F. Perez, S.,  
642 Pierrot, D., Poisson, A., Ríos, A. F., Salisbury, J., Santana-Casiano, J. M., Sarma, V. V. S.  
643 S., Schlitzer, R., Schneider, B., Schuster, U., Sieger, R., Skjelvan, I., Steinhoff, T., Suzuki,  
644 T., Takahashi, T., Tedesco, K., Telszewski, M., Thomas, H., Tilbrook, B., Tjiputra, J.,  
645 Vandemark, D., Veness, T., Wanninkhof, R., Watson, A. J., Weiss, R., Wong, C. S., and  
646 Yoshikawa-Inoue, H.: A uniform, quality controlled Surface Ocean CO<sub>2</sub> Atlas (SOCAT),  
647 Earth Syst. Sci. Data, 5, 125-143, doi:10.5194/essd-5-125-2013, 2013.

648 44. Pierrot, D., Neill, C., Sullivan, L., Castle, R., Wanninkhof, R., Lüger, H., Johannessen, T.,  
649 Olsen, A., Feely, R. A., and Cosca, C. E.: Recommendations for autonomous underway  
650 *p*CO<sub>2</sub> measuring systems and data-reduction routines, Deep-Sea Research Part II, 56,  
651 512-522, 2009.

652 45. Rangama, Y., Boutin, J., Etcheto, J., Merlivat, L., Takahashi, T., Delille, B., Frankignoulle,  
653 M., and Bakker, D. C. E.: Variability of the net air-sea CO<sub>2</sub> flux inferred from shipboard and  
654 satellite measurements in the Southern Ocean south of Tasmania and New Zealand, Journal  
655 of Geophysical Research: Oceans (1978-2012), 110(C9), doi: 10.1029/2004JC002619, 2005.

656 46. Roden, N. P., Shadwick, E. H., Tilbrook, B., and Trull, T. W.: Annual cycle of carbonate  
657 chemistry and decadal change in coastal Prydz Bay, East Antarctica, Marine Chemistry,  
658 155(4), 135-147, 2013.

659 47. Rubin, S.I., Takahashi, T., and Goddard, J.G.: Primary productivity and nutrient utilization  
660 ratios in the Pacific sector of the Southern Ocean based on seasonal changes in seawater  
661 chemistry, Deep-Sea Research I 45, 1211-1234, 1998.

662 48. Sabine, L., Feely, R. A., Gruber, N., Key, R. M., Lee, K., Bullister, J. L., Wanninkhof, R.,  
663 Wong, S., Wallace, D. W. R., Tilbrook, B., Millero, F. J., Peng, T.-H., Kozyr, A., Ono, T.,  
664 and Rios, A. F.: The oceanic sink for anthropogenic CO<sub>2</sub>, Science, 305, 367-371,  
665 doi:10.1126/science.1097403, 2004.

- 666 49. Sarma, V. V. S. S., Saino, T., Sasaoka, K., Nojiri, Y., Ono, T., Ishii, M., Inoue, H. Y., and  
667 Matsumoto, K.: Basin-scale  $p\text{CO}_2$  distribution using satellite sea surface temperature, Chl-a,  
668 and climatological salinity in the North Pacific in spring and summer, *Global*  
669 *Biogeochemical Cycles*, 20, GB3005, doi:10.1029/2005GB002594, 2006.
- 670 50. Shadwick, E. H., Trull, T. W., Thomas, H., and Gibson, J. A. E.: Vulnerability of polar  
671 oceans to anthropogenic acidification: comparison of Arctic and Antarctic seasonal cycles,  
672 *Scientific Reports*, 3: 2339, doi: 10.1038/srep02339, 2013.
- 673 51. Silulwane, N. F., Richardson, A. J., Shillington, F. A., and Mitchell-Innes, B. A.:  
674 Identification and classification of vertical chlorophyll patterns in the Benguela upwelling  
675 system and Angola-Benguela front using an artificial neural network, *South African Journal*  
676 *of Marine Science*, 23, 37-51, 2001.
- 677 52. Smith, N. R., Zhaoqian, D., Kerry, K. R., and Wright, S.: Water masses and circulation in  
678 the region of Prydz Bay Antarctica, *Deep-sea-research*, 31, 1121-1147, 1984.
- 679 53. Smith, N., and Tréguer, P.: *Physical and chemical oceanography in the vicinity of Prydz*  
680 *Bay, Antarctica*, Cambridge University Press, Cambridge, 1994.
- 681 54. Spreen, G., Kaleschke, L., and Heygster, G.: Sea ice remote sensing using AMSR-E 89  
682 GHz channels, *J. Geophys. Res.*, 113, C02S03, doi:10.1029/2005JC003384, 2008.
- 683 55. Sun, W. P., Han, Z. B., Hu, C. Y., and Pan, J. M.: Particulate barium flux and its relationship  
684 with export production on the continental shelf of Prydz Bay, east Antarctica, *Marine*  
685 *Chemistry*, 157, 86-92, 2013.
- 686 56. Sweeney, C., Hansell, D. A., Carlson, C. A., Codispoti, L. A., Gordon, L. I., Marra, J.,  
687 Millero, F. J., Smith, W. O., and Takahashi, T.: Biogeochemical regimes, net community  
688 production and carbon export in the Ross Sea, Antarctica, *Deep Sea Research II*, 47(15-16),  
689 3369-3394, 2000.
- 690 57. Sweeney, C.: The annual cycle of surface water  $\text{CO}_2$  and  $\text{O}_2$  in the Ross Sea: a model for gas  
691 exchange on the continental shelves of Antarctic, *Biogeochemistry of the Ross Sea*,  
692 *Antarctic Research Series*, 78, 295-312, 2002.
- 693 58. Sweeney, C.: The annual cycle of surface water  $\text{CO}_2$  and  $\text{O}_2$  in the Ross Sea: A model for  
694 gas exchange on the continental shelves of Antarctic, *Biogeochemistry of the Ross Sea*,  
695 *Antarctic Research Series*, 78, 295-312, 2002.

- 696 59. Takahashi, T. Feely, R. A., Weiss, R. F., Wanninkhof, R. H., Chipman, D. W., Sutherland, S.  
697 C., and Takahashi, T. T.: Global sea-air CO<sub>2</sub> flux based on climatological surface ocean  
698 *p*CO<sub>2</sub>, and seasonal biological and temperature effects, *Deep-Sea Res. Pt. II*, 49(9-10),  
699 1601-1622, 2002.
- 700 60. Takahashi, T., Sutherland, S. C., Wanninkhof, R., Sweeney, C., Feely, R. A., Chipman, D.  
701 W., Hales, B., Friederich, G., Chavez, F., Sabine, C., Watson, A. J., Bakker, D. C., Schuster,  
702 U., Metzl, N., Yoshikawa-Inoue, H., Ishii, M., Midorikawa, T., Nojiri, Y., Körtzinger, A.,  
703 Steinhoff, T., Hoppema, M., Olafsson, J., Arnarson, T. S., Tilbrook, B., Johannessen, T.,  
704 Olsen, A., Bellerby, R., Wong, C. S., Delille, B., Bates, N. R., and de Baar, H. J. W.:  
705 Climatological mean and decadal change in surface ocean *p*CO<sub>2</sub>, and net sea-air CO<sub>2</sub> flux  
706 over the global oceans, *Deep-Sea Res. Pt. II*, 56(8-10), 554-577, 2009.
- 707 61. Takahashi, T., Sweeney, C., Hales, B., Chipman, D. W., Newberger, T., Goddard, J. G.,  
708 Iannuzzi, R. A., and Sutherland, S. C.: The changing carbon cycle in the Southern Ocean,  
709 *Oceanography*, 25, 26-37, 2012.
- 710 62. Telszewski, M., Chazottes, A., Schuster, U., Watson, A. J., Moulin, C., Bakker, D. C. E.,  
711 González-Dávila, M., Johannessen, T., Körtzinger, A., Lüger, H., Olsen, A., Omar, A.,  
712 Padin, X. A., Ríos, A. F., Steinhoff, T., Santana-Casiano, M., Wallace, D. W. R., and  
713 Wanninkhof, R.: Estimating the monthly *p*CO<sub>2</sub> distribution in the North Atlantic using a  
714 self-organizing neural network, *Biogeoscience*, 6, 1405-1421, 2009.
- 715 63. Thomson, R. E., and Fine, I. V.: Estimating mixed layer depth from oceanic profile data, *J.*  
716 *Atmos. Oceanic Technol.*, 20, 319-329, 2003.
- 717 64. Ultsch, A., and Röske, F.: Self-organizing feature maps predicting sea levels, *Information*  
718 *Sciences*, 144, 91-125, 2002.
- 719 65. Vesanto, J.: *Data Exploration Process Based on the Self-Organizing Map: the Finnish*  
720 *Academies of Technology*, 2002.
- 721 66. Wanninkhof, R.: Relationship between wind speed and gas exchange over the ocean  
722 revisited, *Limnology and Oceanography: Methods*, 12, 351-362, 2014.
- 723 67. Weiss, R. F.: Carbon dioxide in water and seawater: The solubility of a nonideal gas, *Marine*  
724 *Chemistry*, 2, 201-215, 1974.
- 725 68. Worby, A. P., Geiger, C. A., Paget, M. J., Van Woert, M. L., Ackley, S. F., and De Liberty,  
726 T. L.: Thickness distribution of Antarctic sea ice, *Journal of Geophysical Research* 113,

- 727 C05S92, <http://dx.doi.org/10.1029/2007JC004254>, 2008.
- 728 69. Wu, L., Wang, R., Xiao, W., Ge, S., Chen, Z., and Krijgsman, W.: Productivity-climate  
729 coupling recorded in Pleistocene sediments off Prydz Bay (East Antarctica),  
730 *Palaeogeography, Palaeoclimatology, Palaeoecology*, 485, 260-270, 2017.
- 731 70. Xu, S., Chen, L., Chen, H., Li, J., Lin, W., and Qi, D.: Sea-air CO<sub>2</sub> fluxes in the Southern  
732 Ocean for the late spring and early summer in 2009, *Remote Sensing of Environment*, 175,  
733 158-166, 2016.
- 734 71. Yabuki, T., Suga, T., Hanawa, K., Matsuoka, K., Kiwada, H., and Watanabe, T.: Possible  
735 source of the Antarctic Bottom Water in Prydz Bay region, *Journal of Oceanography*, 62,  
736 649-655, doi: 10.1007/s10872-006-0083-1, 2006.
- 737 72. Zeng, J., Nojiri, Y., Nakaoka, S., Nakajima, H., and Shirai, T.: Surface ocean CO<sub>2</sub> in  
738 1990-2011 modelled using a feed-forward neural network, *Geoscience Data Journal*, 2,  
739 47-51, doi: 10.1002/gdj3.26, 2015.
- 740 73. Zeng, J., Mtsunaga, T., Saigusa, N., Shirai, T., Nakaoka, S., and Tan, Z.: Technical note:  
741 Evaluation of three machine learning models for surface ocean CO<sub>2</sub> mapping, *Ocean Sci.*,  
742 13, 303-313, <http://doi.org/10.5194/os-13-303-2017>, 2017.
- 743 74. Zeng, J., Nojiri, Y., Murphy, P. P., Wong, C. S., and Fujinuma, Y.: A comparison of  
744  $\Delta p\text{CO}_2$  distributions in the northern North Pacific using results from a commercial vessel in  
745 1995-1999, *Deep Sea Res., Part II*, 49, 5303-5315, 2002.
- 746